CU Journal of Non-Linear Fluid Mechanics
Vol. 01, No. 02, 2025
https://doi.org/10.11615/cujnlfm.01201-7

Internal Heat Generated Convection in Nanofluids with Rigid Boundaries:Linear and Nonlinear Regimes

P. S. Kruthik *[a] and Ruwaidiah Idris[a]

[a]Special Interest Group for Modelling and Data analytics (SIGMDA), Faculty of Computer Science and Mathematics, Universiti Malaysia Terengganu, Kuala Nerus, 21030, Terengganu, Malaysia

Abstract

This paper investigates the linear and nonlinear stability characteristics of convection driven by internal heat generation in well-dispersed nanoliquids. Water and ethylene glycol are taken as base fluids, each uniformly seeded with nanoparticles of gold, silver, platinum, or diamond. Using mixture theory and phenomenological models, the thermophysical properties of the nanoliquids are incorporated into a modified Rayleigh number that includes a dimensionless parameter F representing nanoparticle loading. In this framework, the Rayleigh number associated with internal heat generation naturally emerges as an eigenvalue. Linear stability is analyzed using a Maclaurin-series expansion, which provides the critical conditions for the onset of convection. For the nonlinear regime, a Fourier–Galerkin procedure is employed to derive a generalized Lorenz system, and a corresponding Ginzburg–Landau equation is obtained to describe amplitude evolution near the convection threshold. This integrated analytical approach offers deeper insight into the behavior of internally heated nanoliquid convection and has potential applications in thermal management and energy system design. The inclusion of high-conductivity noble metal nanoparticles highlights distinct heat transfer and stability responses arising from internal heat generation.

Keywords: Internal heat generation; Convection; Semi-analytical method; Boundary eigenvalue problem; Maclaurin series; Linear stability; Nonlinear stability.

1 Introduction

Internal heat driven convection has been an important topic in fluid mechanics because of its wide relevance in geophysical, astrophysical, and industrial processes. Early experiments by Tritton and Zarraga[1] showed that when a fluid layer is heated internally, convection patterns form in a way similar to classical Bénard convection. Their study further pointed out that this class of convection phenomena has relevance to several real-world systems, such as models of Earth's mantle convection, among others. Following this experimental observation, Roberts[2] carried out a theoretical analysis of a uniformly heated horizontal layer and determined the critical Rayleigh number and the corresponding wave number for the onset of convection. Thirlby[3] later used finite-difference methods to solve the Roberts' results, showing how the Rayleigh and Prandtl numbers shape the flow patterns. Building on that foundation, Schwiderski[4], Peckover and Hutchinson[5], and Gasser and Kazimi[6] clarified issues of stability, boundary conditions, and the role of internal heat generation. Hamabata and Takashima[7] examined

* p5724@pps.umt.edu.my

the influence of rotation with internal heat generation. Tasaka and Takeda[8] along with Kuznetsov and Nield[9] analyzed non-uniform heat source distributions. Their results showed that internal heating interacts strongly with stabilizing mechanisms such as rotation which can delay convection depending on the configuration. More recent high-Rayleigh-number simulations by Goluskin and van der Poel[10], and Wang et al.[11] gave valuable scaling laws linking mean temperature, flow intensity, and heat transport. Deepika et al.[12] examined the onset of thermal convection in a fluid-saturated Darcy–Brinkman porous medium in the presence of throughflow and uniform internal heating.

Recent works have moved beyond ordinary liquids and an extensive study has begun on examining nanofluids base fluids mixed with nanoparticles that can noticeably enhance heat transfer. Cooling efficiency is critical in both electrical and mechanical systems, and the industires in the earlier ages mainly relied on air or water as a cooling source. Because of their potential applications, the studies were eventually conducted with suspending micron-sized solid particles with high thermal conductivity. Although this approach did enhance heat transfer, the particles often settled, clustered, or clogged flow passages, which limited practical use. Moving to nanoparticles helped overcome these problems their much smaller size offers better suspension stability and lowers the risk of blockage while still enhancing thermal transport.

Introducing nanoparticles changes key fluid properties viscosity, density, and thermal conductivity which directly affect convective behaviour. As a result, convection in internally heated nanofluids presents new dynamics and continues to attract attention. Choi[13] was the first to introduce the concept of nanofluids, describing how dispersing nanoparticles in conventional base fluids could significantly enhance their thermal conductivity. Building on these early developments, Eastman et al.[14] demonstrated that a significant increase in the thermal conductivity of ethylene-glycol-based nanofluids this encouraged other researchers to carry more research on this and later, Das et al.[15] expanded this work by examining the influence of temperature on conductivity enhancement. Buongiorno[16] later introduced a detailed framework for convective transport in nanofluids, highlighting Brownian motion and thermophoresis as the key slip mechanisms. Together, these studies opened the door to a broad range of applications from microelectronics cooling to solar thermal technologies and helped establish nanofluids as a viable option for improved thermal management.

Rayleigh–Bénard convection (RBC) in nanofluids is often analyzed using two main approaches the Khanafer–Vafai–Lightstone(KVL) single-phase model[17] and the Buongiorno two-phase model[16]. Siddheshwar et al. [18], [19] showed that both models provide thermodynamically consistent results and accurately describe the enhancement of heat transfer in nanofluids. Recently Kanchana and Laroze[20] investigated the Rayleigh–Bénard convection of a water–alumina nanofluid in the presence of an internal heat source/sink and analyzed the onset of chaotic behavior using a generalized Lorenz model. They found that addition of nanoparticles and heat sinks were shown to delay or suppress chaotic convection, stabilizing thermally driven nanofluids.

The semi-analytical method based approach for obtaing the estimate of the eigenvalue is thoroughly discussed in Siddheshwar et al. [21], [22], [23], we adapt similar methodology to obtain the eigenvalue for our problem. While most previous studies have focused

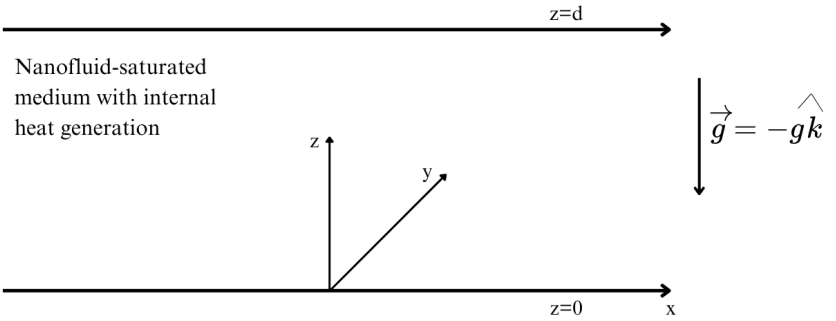

Figure 1: Physical configuration of the problem.

on common oxide-based nanofluids such as alumina or copper, the present investigation uniquely explores gold, silver, diamond, and platinum nanoparticles, whose thermal properties produce distinctive convection and heat transfer characteristics under internal heat generation. The existing literature suggests that internal-heat–driven convection, in which the Rayleigh number appears as an eigenvalue associated with heat generation, has not been thoroughly examined particularly for rigid–rigid boundary conditions in the context of nanofluids.

2 Mathematical Formulation

We consider a horizontal layer of fluid of with a thickness d, bounded between two rigid parallel plates located at $z = 0$ and $z = d$. We consider the nanoliquids properties such as density as ρ_{nl}, dynamic viscocsity as μ_{nl}, thermal diffusivity as χ_{nl}, and coefficient of thermal as expansion β_{nl}. The velocity is taken as $\vec{q} = (u, 0, w)$. A uniform internal heat source, Q, in the energy equation to represents volumetric uniform heating within the layer. The subscript *nl* refers to the nanoliquid phase, while *np* denotes the nanoparticle phase. The governing equations are modeled under the Boussinesq approximation, whereby density is treated as constant except in the buoyancy term that appears in conjunction with gravity.
The governing equations are as follows:

$$\nabla . \vec{q} = 0, \tag{1}$$

$$\rho_{nl}\left[\frac{\partial \bar{q}}{\partial t} + (\bar{q}\cdot\nabla)\bar{q}\right] + \nabla p - \mu_{nl}\nabla^2\bar{q} + \rho_{nl}\left[1 - \beta_{nl}(T - T_0)\right]g\mathbf{k} = 0, \tag{2}$$

$$\frac{\partial T}{\partial t} + (\bar{q}\cdot\nabla)T - \chi_{nl}\nabla^2 T - Q = 0, \tag{3}$$

$$\left.\begin{aligned} \frac{\mu_{nl}}{\mu_l} &= \frac{1}{(1-\alpha)^{2.5}}, \\ \frac{k_{nl}}{k_l} &= \frac{\left(\frac{k_{np}}{k_l}+2\right) - 2\alpha\left(1 - \frac{k_{np}}{k_l}\right)}{\left(\frac{k_{np}}{k_l}+2\right) + \alpha\left(1 - \frac{k_{np}}{k_l}\right)} \end{aligned}\right\}, \tag{4}$$

$$\left.\begin{aligned} \chi_{nl} &= \frac{k_{nl}}{(\rho C_p)_{nl}}, \\ \frac{\rho_{nl}}{\rho_l} &= (1-\alpha)+\alpha\frac{\rho_{np}}{\rho_l}, \\ (\rho C_p)_{nl} &= (1-\alpha)+\alpha\frac{(\rho C_p)_{np}}{(\rho C_p)_l}, \\ (\rho\beta)_{nl} &= (1-\alpha)+\alpha\frac{(\rho\beta)_{np}}{(\rho\beta)_l} \end{aligned}\right\}. \tag{5}$$

In Eqs. (1)-(5), Eq.(1) is the law of conservation of mass [23], Eq.(2) is the law of conservation of linear momentum [23], Eq.(3) is the law of conservation of energy [23], Eq.(4) are the phenomenological laws [18] and Eq.(5) are the mixture theory laws [18] which govern the system. Considering Eqs.(1)-(3) in component form we get

$$\frac{\partial u}{\partial x}+\frac{\partial v}{\partial y}=0, \tag{6}$$

$$\rho_{nl}\left[\frac{\partial u}{\partial t}+u\frac{\partial u}{\partial x}+\omega\frac{\partial u}{\partial z}\right]=-\frac{\partial p}{\partial x}+\mu_{nl}\nabla^2 u \tag{7}$$

$$\rho_{nl}\left[\frac{\partial w}{\partial t}+u\frac{\partial w}{\partial x}+\omega\frac{\partial w}{\partial z}\right]=-\frac{\partial p}{\partial z}+\mu_{nl}\nabla^2 w-\rho_{nl}[1-\beta_{nl}(T-T_o)], \tag{8}$$

$$\frac{\partial T}{\partial t}+\left(u\frac{\partial T}{\partial x}+\omega\frac{\partial T}{\partial z}\right)=\chi_{nl}\,\nabla^2 T+Q. \tag{9}$$

By substituting Eq. (6) and then taking the partial derivative of Eq. (7) with respect to z and of Eq. (8) with respect to x, and finally subtracting these expressions, the pressure term is eliminated. Taking the velocity and temperature in the basic state to be $(u_b,w_b)=(0.0), T_b(z)$ and $\rho_b(z)$, we obtain the basic state solution in the form:

$$T_b(z)=\frac{1-z^2}{2}\Bigg\}, \tag{10}$$

We introduce perturbations to the basic state by expressing them in the form:

$$(u,w)=(u_b+u',w_b+w'),\quad T=T_b(z)+T', \tag{11}$$

where prime indicates perturbed quantity.We define the stream function, ψ, such that:

$$u'=-\frac{\partial\psi'}{\partial z}\ \text{ and } w'=\frac{\partial\psi'}{\partial x}, \tag{12}$$

and these expressions automatically satisfy Eq. (1) in its perturbed form. We introduce the following nondimensional scaling for the governing equations. This scaling is particularly suitable for analyzing convection regimes where the internal heat generation term appears in the Rayleigh number:

$$(X,Z)=\left(\frac{x}{d},\frac{z}{d}\right),\tau=\frac{t}{d^2/\chi_l},\Psi=\frac{\psi'}{\chi_l},\Theta=\frac{T'}{Qd^2/\chi_l}. \tag{13}$$

The dimensionless form of the equations, that we get are:

$$\frac{1}{Pr_{nl}}\left[\frac{\partial}{\partial\tau}\left(\nabla^2\Psi\right)+\left(\frac{\partial\Psi}{\partial X}\frac{\partial}{\partial Z}-\frac{\partial\Psi}{\partial Z}\frac{\partial}{\partial X}\right)\nabla^2\Psi\right]=a_1\nabla^4\Psi+Ra_{nl}a_1^3\frac{\partial\Theta}{\partial X}, \tag{14}$$

$$\frac{\partial\Theta}{\partial\tau}+\frac{1}{Pr_{nl}}\left(\frac{\partial\Psi}{\partial X}\frac{\partial}{\partial Z}-\frac{\partial\Psi}{\partial Z}\frac{\partial}{\partial X}\right)\Theta=a_1\nabla^2\Theta+Z\frac{\partial\Psi}{\partial X}, \tag{15}$$

where $Pr_{nl}=\frac{\mu_{nl}}{\rho_{nl}\chi_l}$ is the Prandtl number for the nanoliquid, $Ra_{nl}=\frac{(\rho\beta)_{nl}gQd^5}{\left(\mu\chi^2\right)_{nl}}$ is the Rayleigh number for the nanoliquid, here, X and Z represent the nondimensional horizontal and vertical coordinates, respectively. The variable τ denotes the nondimensional time, Ψ is the nondimensional stream function, and Θ is the nondimensional temperature field. The parameter $a_1=\chi/\chi_l$ corresponds to the ratio of thermal diffusivities.
Considering Eqs. (14)-(15) for the rigid-rigid boundary conditions:

$$\begin{aligned}&\frac{\partial\Psi}{\partial X}=0, \qquad \frac{\partial}{\partial Z}\left(\frac{\partial\Psi}{\partial X}\right)=0, \qquad \frac{\partial\Theta}{\partial Z}=0, \quad \text{when } Z=0,\\ &\frac{\partial\Psi}{\partial X}=0, \qquad \frac{\partial}{\partial Z}\left(\frac{\partial\Psi}{\partial X}\right)=0, \qquad \Theta=0, \quad \text{when } Z=1.\end{aligned} \tag{16}$$

The lower surface imposes an adiabatic condition, while the upper boundary is maintained isothermal.

2.1 Linear Stability Analysis

Assuming, PES(principle of exchange of stabilities) is valid and we make use of the normal-mode form in the following way:

$$\left.\begin{aligned}\Psi(X,Z)&=\sin(bX)F(Z),\\ \Theta(X,Z)&=\cos(bX)G(Z)\end{aligned}\right\}, \tag{17}$$

where $F(Z)$ and $G(Z)$ are determined by the boundary conditions in Eq. (16), and b denotes the wave number associated with a longitudinal roll. Substituting Eq. (17) into the linearized forms of Eqs. (14) and (15) leads to:

$$a_1(D^2-b^2)^2F=a_1^3b^2Ra_{nl}G, \tag{18}$$

$$a_1(D^2-b^2)G=-ZF, \tag{19}$$

where $D=\partial/\partial Z$. Eqs.(18) and (19) are solved to the boundary conditions obtained from Eq.(17) and Eq.(16) are:

$$F=DF=0 \quad \text{and} \quad DG=0 \quad \text{at } Z=0, \tag{20a}$$

$$F=DF=0 \quad \text{and} \quad G=0 \quad \text{at } Z=1. \tag{20b}$$

Equations (18)-(19) is a boundary eigenvalue problem (BEVP), this is transformed to an initial problem (IVP). The procedure adopted here follows the approach outlined

by Siddheshwar et al. [21]. Accordingly, the following missing initial condition is introduced:

$$D^2F(0)=\tilde{\gamma},\quad D^3F(0)=\tilde{\alpha},\quad G`(0)=\tilde{\beta}. \tag{21}$$

Only three conditions are supplied at the right boundary, while four unknown parameters appear in the formulation. To address this, we normalize the initial data through $F_1=F/\tilde{\gamma}$ and $G_1=G/\tilde{\gamma}$, leading to the following scaled initial value problem (IVP):

$$a_1(D^2-b^2)^2F_1=a_1^3b^2Ra_{nl}G_1, \tag{22}$$

$$a_1\left(D^2-b^2\right)G_1=-ZF_1, \tag{23}$$

along with the initial condition (20a) and the three right-end boundary condition(REBC) (20b). The REBC is replaced by the conditions given in Eq. (21). The Maclaurin series solutions corresponding to Eqs.(22) and (23) are then expressed as:

$$\left.\begin{aligned}F_1(Z;\tilde{\alpha},\tilde{\beta},Ra)&=\sum_{n=0}^{\infty}c_nZ^n,\\ G_1(Z;\tilde{\alpha},\tilde{\beta},Ra)&=\sum_{n=0}^{\infty}d_nZ^n\end{aligned}\right\}. \tag{24}$$

The substitution of Eq.(24) in Eqs.(22) yields the recurrence relations for the Maclaurin constants c_n and d_n as follows:

$$a_1(k+4)(k+2)(k+1)c_{k+4}=\left[2b^2(k+2)(k+1)c_{k+2}-b^4c_k\right]+a_1^3b^2Ra_{nl}d_k,\quad k=0(1)\infty \tag{25}$$

$$a_1(k+2)(k+1)d_{k+4}=a_1b^2d_k-\sum_{l=0}^{k}\delta_{1l}c_{k-l},\quad k=0(1)\infty \tag{26}$$

The initial Maclaurin coefficients obtained from Eqs. (25) and (26) are

$$c_0=0,\quad c_1=0,\quad c_2=\tfrac{1}{2},\quad c_3=\tfrac{\tilde{\alpha}}{6},\quad d_0=\tilde{\beta},\quad d_1=0.$$

The remaining terms of the expansions follow from the recurrence formulas in Eqs. (25) and (26). Using these relations, the corresponding series solution takes the form:

$$F_1(Z;\tilde{\alpha},\tilde{\beta},Ra)=\frac{Z^2}{2}+\frac{\tilde{\alpha}}{6}Z^3+\frac{b^2+a_1^2b^2Ra_{nl}\tilde{\beta}}{24}Z^4+\frac{b^2\tilde{\alpha}+6\tilde{\alpha}}{120}Z^5 +\cdots \text{ upto 25 terms, TE}=o[Z^{26}], \tag{27}$$

$$G_1(Z;\tilde{\alpha},\tilde{\beta},Ra)=\tilde{\beta}+\tfrac{1}{2}\tilde{\alpha}^2\tilde{\beta}Z^2+\tfrac{1}{24}b^4\tilde{\beta}Z^4-\frac{Z^5}{40a_1}+\cdots \text{ upto 25 terms, TE}=o[Z^{26}], \tag{28}$$

where TE means truncation error. By substituting Eqs. (27) and (28) into the remaining right–end boundary condition given in Eq. (20b), a set of three nonlinear algebraic

equations in the unknowns $\tilde{\alpha}$, $\tilde{\beta}$, and $Ra_{nl}(b)$ is obtained. These equations are solved using the multivariable Newton–Raphson method. Initial estimates for the Rayleigh number and for a suitable interval of wavenumber values are taken from the single–term Galerkin approximation. The wavenumber is then varied over this interval to determine the minimum value of the Rayleigh number, denoted $Ra_{nl,c}$, along with the corresponding critical wavenumber b_c. The accuracy of the series expansions in Eqs. (27) and (28) depends on the number of terms retained, and at least 25 terms are required to achieve accuracy to three significant digits.

2.2 Weakly Nonlinear Stability Analysis

A minimal Fourier-Galerkin expansion is adopted for representing the velocity and temperature fields.

$$\Psi(X,Z,\tau) = \frac{b_c}{m}\sqrt{\frac{\mathscr{I}_1\mathscr{I}_2}{\mathscr{I}_3\mathscr{I}_4}}\mathscr{A}(\tau)\sin(b_cX)F_1(Z), \tag{29}$$

$$\Theta(X,Z,\tau) = \frac{b_c\,Ra_{nl}\,Q_2}{mQ_1}\sqrt{\frac{\mathscr{I}_1\mathscr{I}_2}{\mathscr{I}_3\mathscr{I}_4}}\mathscr{B}(\tau)\cos(b_cX)G_1(Z) - \frac{b_c\,Ra_{nl}\,Q_2\mathscr{I}_1}{m\,Q_1\mathscr{I}_2}\mathscr{C}(\tau)H(Z), \tag{30}$$

where,

$$\left.\begin{aligned}
&\mathscr{I}_1 = \int_0^1 F_1G_1H'\,dZ, \quad \mathscr{I}_2 = \int_0^1 F_1'G_1H\,dZ, \quad \mathscr{I}_3 = \int_0^1 G_1^2\,dZ,\\
&\mathscr{I}_4 = -\int_0^1 H^2\,dZ, \mathscr{I}_5 = \int_0^1 G_1G_1''\,dZ, \mathscr{I}_6 = \int_0^1 HH''\,dZ, \quad m = \frac{\mathscr{I}_5 - b_c^2\mathscr{I}_3}{\mathscr{I}_3},\\
&Q_1 = \frac{\int_0^1 F_1F_1''''\,dZ - 2b_c^2\int_0^1 F_1F_1''\,dZ + b_c^4\int_0^1 F_1^2\,dZ}{b_c^2\int_0^1 F_1^2\,dZ - \int_0^1 F_1F_1''''\,dZ},\\
&Q_2 = \frac{b_c\int_0^1 F_1G_1\,dZ}{b_c^2\int_0^1 F_1^2\,dZ - \int_0^1 F_1F_1''''\,dZ}
\end{aligned}\right\}. \tag{31}$$

The terms $F_1(Z)$ and $G_1(Z)$ are defined in the Eqs.(27) and (28). The function $H(Z)$ is given by

$$H(Z) = F_1'(Z)G_1(Z), \tag{32}$$

where the prime on $F(Z)$ denotes the Z-derivative. The terms $\mathscr{A}(\tau), \mathscr{B}(\tau)$ and $\mathscr{C}(\tau)$ describe time-dependent amplitudes. In Eqs.(29) and (30), the scaling used for the amplitudes is a modified version of those commonly applied in the classical Lorenz model. The modification ensures that the Lorenz model remains structurally similar to the classical version.
The eigenfunctions employed in Eqs. (29) and (30) are

$$\begin{aligned}
E_F(X,Z) &= \sin(bX)\,F(Z),\\
E_G(X,Z) &= \cos(bX)\,G(Z),\\
E_H(Z) &= H(Z),
\end{aligned} \tag{33}$$

where $E_H(Z)$ represents the convective mode, while $E_F(X,Z)$ and $E_G(X,Z)$ arise from the linear analysis. These eigenfunctions satisfy the orthogonality relations

$$\begin{aligned} \langle\langle E_F^2 \rangle\rangle \neq 0, \qquad \langle\langle E_G^2 \rangle\rangle \neq 0, \qquad \langle\langle E_H^2 \rangle\rangle \neq 0, \\ \langle\langle E_F E_G \rangle\rangle = 0, \qquad \langle\langle E_F E_H \rangle\rangle = 0, \qquad \langle\langle E_G E_H \rangle\rangle = 0, \end{aligned} \tag{34}$$

with the angular bracket is defined by

$$\langle\langle f,g \rangle\rangle = \int_0^{\frac{2\pi}{b}} \int_0^1 f(X,Z)\, g(X,Z)\, dZ\, dX.$$

Substituting Eqs. (29) and (30) into Eqs. (18) and (19), and projecting the resulting expressions onto the Eigenfunctions E_F, E_G, and E_H and using the orthogonality conditions in Eq. (34), yields the generalized Lorenz model.

$$\frac{d\mathscr{A}}{d\tau} = Pr^*[\mathscr{B} - \mathscr{A}], \tag{35}$$

$$\frac{d\mathscr{B}}{d\tau} = r^*\mathscr{A} - \mathscr{A}\mathscr{C} - \mathscr{B}, \tag{36}$$

$$\frac{d\mathscr{C}}{d\tau} = -m^*\mathscr{C} + \mathscr{A}\mathscr{B}, \tag{37}$$

where

$$m^* = \frac{a_1}{\mathscr{I}_1} \frac{\int_0^1 HH''\, dZ}{\int_0^1 H^2\, dZ}, \quad r^* = \frac{Ra_{nl}}{Ra_{nl_c}}, \quad Pr^* = PrQ_1.$$

To derive the Ginzburg–Landau equation from the Lorenz model, we first rewrite $\mathscr{B}$ and $\mathscr{C}$ in terms of $\mathscr{A}$ using Eqs. (36) and (37):

$$\mathscr{B} = \mathscr{A} + \frac{1}{Pr^*} \frac{d\mathscr{A}}{d\tau}, \tag{38}$$

$$\mathscr{C} = \frac{1}{\mathscr{A}} \left[(r^* - 1)\mathscr{A} - \left(\frac{1}{Pr^*} + 1 \right) \frac{d\mathscr{A}}{d\tau} - \frac{1}{Pr^*} \frac{d^2\mathscr{A}}{d\tau^2} \right]. \tag{39}$$

Substituting Eqs. (38) and (39) into Eq. (37) and neglecting the higher–order terms $\frac{d^3\mathscr{A}}{d\tau^3}$, $\left(\frac{d^2\mathscr{A}}{d\tau^2}\right)\left(\frac{d\mathscr{A}}{d\tau}\right)$, and $\mathscr{A}\left(\frac{d^2\mathscr{A}}{d\tau^2}\right)$, we obtain the Ginzburg-Landau equation

$$\frac{d\mathscr{A}}{d\tau} = \left(\frac{Pr^*}{1 + Pr^*} \right) \frac{1}{m^*} \left[m^*(r-1)\mathscr{A} - \mathscr{A}^3 \right]. \tag{40}$$

Equation (40) is a Bernoulli equation in $\mathscr{A}$. With the initial condition $\mathscr{A}(0) = \mathscr{A}_0 = 1$, the solution is

$$\mathscr{A}(\tau) = \left[\frac{1}{m^*(r^* - 1)} + \left(1 - \frac{1}{m^*(r^* - 1)} \right) e^{-\frac{2(r^* - 1)}{1 + \mathrm{Pr}^*} \tau^*} \right]^{-\frac{1}{2}}. \tag{41}$$

2.3 Estimate of the Nusselt Number

To estimate the heat transport, we use the thermal Nusselt number, Nu_{nl}, which is defined by:

$$Nu_{nl}(\tau) = \frac{\text{Heat transport by (conduction + convection)}}{\text{Heat transport by conduction}}. \tag{42}$$

Using Fourier's first law, we get:

$$\text{Heat transport by conduction} = \left[k_l \int_0^{2\pi} \frac{\partial T_b}{\partial Z} dX\right]_{Z=0}, \tag{43}$$

$$\text{Heat transport by convection} = \left[k_{nl} \int_0^{2\pi} \frac{\partial \Theta}{\partial Z} dX\right]_{Z=0}. \tag{44}$$

Substituting the non-dimensional form of the basic state solution of temperature from Eq.(10) in Eq.(43), substituting Eq.(30) in Eq.(44) and completing the integration, we get

$$Nu_{nl}(\tau^*) = 1 + \frac{k_{nl}}{k_l} H''(0) \mathscr{C}(\tau^*), \tag{45}$$

where $\mathscr{C}(\tau^*)$ in terms of $\mathscr{A}(\tau^*)$ is given by Eq.(39).

3 Validation of the study

By setting the nanoparticle volume fraction to zero, the present study reduces to a clear Newtonian fluid case. In this case for the linear analysis, the results of Roberts[2] are exactly recovered from the present formulation, with the critical Rayleigh number matching up to three-digit numerical accuracy.

4 Results and discussion

The present study analyzes both the linear and nonlinear stability of internal heat generated convection in a well dispersed nanoliquids. Nanoliquids are formulated with water and ethylene glycol as base fluids, each containing four different nanoparticle types, are examined using thermophysical properties derived from mixture theory. The work explores how nanoparticle concentration, the choice of base fluid, and parameters such as effective thermal conductivity, specific heat capacity, and thermal expansion influence the onset of convection and the resulting heat transport. Comparisons are made across various nanoliquid combinations by evaluating changes in the modified Rayleigh number and the Nusselt number.

In this study, the nanofluid Rayleigh number is determined using effective thermophysical properties based on mixture theory, phenomenological models, and experimental data from previous works. Tables 1 and 2 list the properties of the base fluids and nanoparticles used to develop the modified Rayleigh number. These values serve as the basis for further calculations. Using the relations in Eqs.(4)–(5), a dimensionless factor

F was introduced to adjust the Rayleigh number for the influence of nanoparticle concentration and fluid characteristics. The final computed results, shown in Table 3, were obtained from these models. The factor $F = \frac{(1-\alpha^{2.5})(\rho\beta)_{nl}}{a_1\rho_l\beta_l}$ governs the critical threshold for the onset of convection.

Table 5 shows that the factor, F, changes noticeably among the eight nanoliquids studied and has a strong influence on the onset of convection. Since F is inversely related to the critical Rayleigh number, larger values of F indicate earlier onset of convection, while smaller values delay it because of stronger viscous and diffusive resistance. At a 2% volume fraction, water–gold has the highest F value (0.8945), followed by water–platinum and water–silver, suggesting faster onset of convective. In comparison, EG–diamond has one of the lowest F values (0.8729), showing greater system stability. Increasing the concentration to 3% causes a slight drop in F across all nanoliquids for instance, Water–Gold decreases from 0.8945 to 0.8459, and EG–Diamond from 0.8729 to 0.8155. Although Diamond nanoparticle has high thermal conductivity, the rise in viscosity with more particles reduces F and slows convection. Because ethylene glycol is naturally more viscous than water, EG-based nanofluids show smaller F values overall. Among them, EG–silver and EG–gold retain relatively lower F values, while EG–diamond and EG–platinum show higher ones, indicating a weaker tendency for convection as concentration increases.

The Nusselt number trends across the eight nanoliquids show how particle conductivity, base fluid properties, and volume fraction affect the heat transfer. Nanoliquids with relatively higher thermal conductivity like diamond and silver gives us larger Nusselt numbers, better heat transport. This trend is consistent in both water-based and EG-based nanoliquids, with diamond nanofluids showing the most heat transfer this can be observed in Table-6 and Figs. 2 and 3. Gold- and platinum-based nanoliquids, on the other hand, show smaller Nusselt numbers, especially when dispersed in ethylene glycol, where higher viscosity limits the flow. Water-based nanofluids generally have better heat tranfer than those using ethylene glycol because of water's lower viscosity and higher thermal diffusivity.

The current analysis reveals that the thermal properties of nanoliquids are governed by enhanced conductivity and increased viscosity. If the nanoparticles addition in a minial quantity is carried out the we can see the positive effects such as improved heat transfer but if the addition of the nanoparticle is beyond a certai volume fraction then there is a possibility of agglomeration. To maximize heat transport, it is crucial to select nanoparticle and base liquid pairs that demonstrate a higher F value at their specific optimal concentration.

Table 1: Values of thermophysical properties of Diamond, Silver, Copper, Gold, Platinum, Alumina nanoparticles at room temperature (300K).

Quantity	Diamond[24]	Silver[24]	Gold[24]	Platinum[24]
Density (ρ_{np}) [kg/m^3]	3500	10500	19300	2145
Thermal expansion coefficient (β_{np}) $[K^{-1} \times 10^5]$	1	1.89	1.42	0.89
Specific heat $(C_{P_{np}})$ [J/kgK]	509	235	129	133
Thermal conductivity (k_{np}) [W/mK]	2300	429	317	71.6

Table 2: Thermophysical properties of twelve nanoliquids for $\alpha = 3\%$.

Nanoliquids	ρ_{nl}	k_{nl}	μ_{nl}	$(C_p)_{nl}$	$\beta_{nl} \times 10^{-5}$	$\alpha_{nl} \times 10^7$	Pr_{nl}
Water–Diamond	1072.19	0.669829	0.00096	3819.59	19.0414	1.6356	5.48
Water–Silver [18]	1282.19	0.669626	0.00096	3210.06	16.3052	1.62692	4.6
Water–Gold	1546.19	0.669538	0.00096	2662.4	13.6679	1.62645	3.82
Water–Platinum	1610.69	0.668397	0.00096	2562.55	12.9657	1.61939	3.64
EG–Diamond	1185.97	0.275374	0.016942	2246.25	59.3337	1.03369	138.83
EG–Silver [18]	1395.97	0.275339	0.016942	1923.08	50.7592	1.02564	118.33
EG–Gold	1659.97	0.275324	0.016942	1617.64	42.0852	1.02533	99.34
EG–Platinum	1724.47	0.275129	0.016942	1563.45	41.0768	1.02046	96.28

Table 3: Thermophysical properties of ten nanoliquids for $\alpha = 2\%$.

Nanoliquids	ρ_{nl}	k_{nl}	μ_{nl}	$(C_p)_{nl}$	$\beta_{nl} \times 10^{-5}$	$\alpha_{nl} \times 10^7$	Pr_{nl}
Water–Diamond	1047.16	0.6505	0.000936	3933.67	19.663	1.5792	5.66
Water–Silver	1187.16	0.650367	0.000936	3481.33	17.6196	1.57364	5.01
Water–Gold	1363.16	0.650309	0.000936	3032.18	15.4556	1.57333	4.36
Water–Platinum	1406.16	0.649564	0.000936	2944.62	14.8647	1.56877	4.24
EG–Diamond	1162.11	0.267423	0.016513	2308.19	61.1449	1.00043	142.04
EG–Silver	1302.11	0.267401	0.016513	2063.42	54.8218	0.99154	127.43
EG–Gold	1478.11	0.267391	0.016513	1818.02	48.3965	0.99504	112.28
EG–Platinum	1521.11	0.267264	0.016513	1771.41	46.919	0.99188	109.45

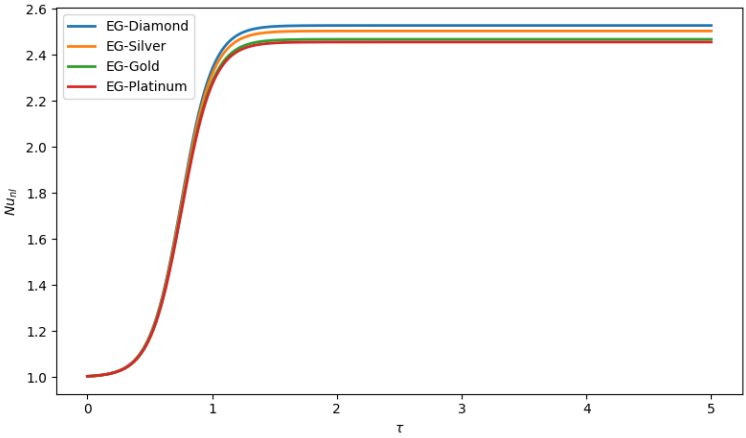

Figure 2: Plot of Nu vs τ for different nanoliquids with $\alpha = 2\%$.

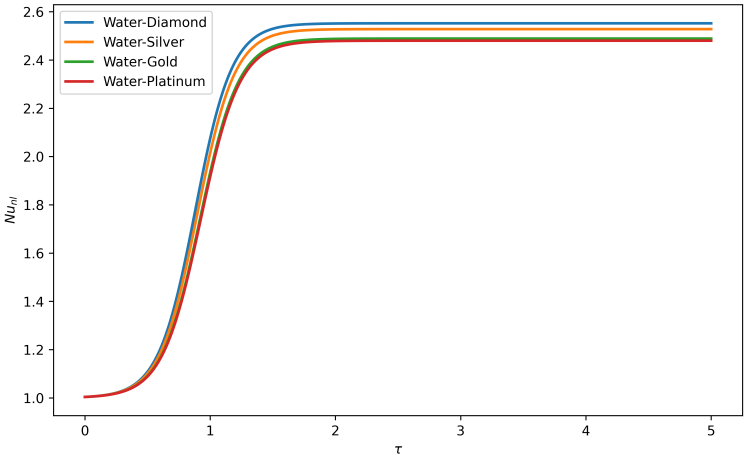

Figure 3: Plot of Nu vs τ for different nanoliquids with $\alpha = 2\%$.

Table 4: Values of thermophysical properties of water and ethylene glycol at room temperature (300K).

Quantity	Water[18]	Ethylene glycol[18]
Density (ρ_f) [kg/m^3]	997.1	1114.4
Thermal expansion coefficient (β_f) [$K^{-1} \times 10^5$]	21	65
Specific heat (C_{pf}) [J/kgK]	4179	2415
Thermal conductivity (k_f) [W/mK]	0.613	0.252
Dynamic viscosity (μ_f) [kg/m-s]	0.00089	0.0157

Table 5: Values of the factor, F, for twelve nanoliquids.

Nanoliquids	$\alpha = 0.02$	$\alpha = 0.03$
Water–Diamond	0.870928	0.812668
Water–Silver	0.887884	0.836624
Water–Gold	0.894478	0.845949
Water–Platinum	0.889997	0.839606
EG–Diamond	0.87292	0.815457
EG–Silver	0.881511	0.827587
EG–Gold	0.883556	0.830487
EG–Platinum	0.884307	0.83152

Table 6: Values of the Nusselt number, Nu_{nl}, for twelve nanoliquids for $\alpha = 0.02$.

Nanoliquids	Nu_{nl} $(2 \times Ra_{c,nl})$	Nu_{nl} $(5 \times Ra_{c,nl})$
Water–Diamond	1.9239	2.4649
Water–Silver	1.9104	2.4401
Water–Gold	1.8961	2.4121
Water–Platinum	1.8909	2.4080
EG–Diamond	1.9721	2.5528
EG–Silver	1.9556	2.5284
EG–Gold	1.9275	2.4847
EG–Platinum	1.9253	2.4821

5 Conclusion

The conclusions from the study can be listed as below:

- The factor F varies significantly across nanoliquids and determines the onset of convection—water-based nanofluids show earlier onset of convection than EG-based ones due to lower viscosity.
- Heat transfer increases with high-conductivity nanoparticles (e.g., diamond, silver), while higher viscosity in EG reduces the Nusselt number and overall heat transport.
- Optimal nanoparticle concentration is crucial—small additions enhance heat transfer, but higher volume fractions reduce F, increase viscosity, and may lead to agglomeration.

References

[1] Tritton D. J. and Zarraga M. N., "Convection in horizontal layers with internal heat generation. Experiments", *Journal of Fluid Mechanics*, vol. 30, (1), pp. 21–31, 1967.

[2] Roberts P. H., "Convection in horizontal layers with internal heat generation. Theory", *Journal of Fluid Mechanics*, vol. 30, (1), pp. 33–49, 1967.

[3] Thirlby R, "Convection in an internally heated layer", *Journal of Fluid Mechanics*, vol. 44, (4), pp. 673–693, 1970.

[4] Schwiderski E. W., "Bifurcation of convection in internally heated fluid layers", *Physics of Fluids*, vol. 15, (11), pp. 1882–1898, 1972.

[5] Peckover R. S. and Hutchinson I. H., "Convective rolls driven by internal heat sources", *Physics of Fluids*, vol. 17, (7), pp. 1369–1371, 1974.

[6] Gasser R. and Kazimi M., "Onset of convection in a porous medium with internal heat generation", *Journal of Heat Transfer*, vol. 98, (1), pp. 49–54, 1976.

[7] Hamabata H. and Takashima M., "The effect of rotation on convective instability in a horizontal fluid layer with internal heat generation", *Journal of the Physical Society of Japan*, vol. 52, (12), pp. 4145–4151, 1983.

[8] Tasaka Y. and Takeda Y., "Effects of heat source distribution on natural convection induced by internal heating", *International Journal of Heat and Mass Transfer*, vol. 48, (6), pp. 1164–1174, 2005.

[9] Kuznetsov A. and Nield D., "The effect of spatially nonuniform internal heating on the onset of convection in a horizontal fluid layer", *Journal of Heat Transfer*, vol. 138, (6), p. 062 503, 2016.

[10] Goluskin D. and Poel E. P. Van der, "Penetrative internally heated convection in two and three dimensions", *Journal of Fluid Mechanics*, vol. 791, R6, 2016.

[11] Wang Q., Lohse D., and Shishkina O., "Scaling in internally heated convection: A unifying theory", *Geophysical Research Letters*, vol. 48, (4), e2020GL091198, 2021.

[12] Deepika N., Narayana P. A. L., and Hill A. A., "Onset of Darcy-Brinkman convection with a uniform internal heat source and vertical throughflow", *International Journal of Thermal Sciences*, vol. 117, pp. 136–144, 2017.

[13] Choi S. and Eastman J., "Enhancing thermal conductivity of fluids with nanoparticles", *Proceedings of the ASME International Mechanical Engineering Congress and Exposition*, vol. 66, Jan. 1995.

[14] Eastman J. A., Choi S., Li S., Yu W, and Thompson L. J., "Anomalously increased effective thermal conductivities of ethylene glycol-based nanofluids containing copper nanoparticles", *Applied Physics Letters*, vol. 78, (6), pp. 718–720, 2001.

[15] Das S. K., Putra N. S. D., Thiesen P., and Roetzel W., "Temperature dependence of thermal conductivity enhancement for nanofluids", *Journal of Heat Transfer*, vol. 125, (4), pp. 567–574, 2003.

[16] Buongiorno J., "Convective transport in nanofluids", *Journal of Heat Transfer*, vol. 128, (3), pp. 240–250, Aug. 2005.

[17] Khanafer K., Vafai K., and Lightstone M., "Buoyancy-driven heat transfer enhancement in a two-dimensional enclosure utilizing nanofluids", *International Journal of Heat and Mass Transfer*, vol. 46, (19), pp. 3639–3653, 2003.

[18] Siddheshwar P. G. and Meenakshi N, "Amplitude equation and heat transport for Rayleigh–Bénard convection in Newtonian liquids with nanoparticles", *International Journal of Applied and Computational Mathematics*, vol. 3, (1), pp. 271–292, 2017.

[19] Siddheshwar P. G., Kanchana C, Kakimoto Y, and Nakayama A., "Steady finite-amplitude Rayleigh–Bénard convection in nanoliquids using a two-phase model: Theoretical answer to the phenomenon of enhanced heat transfer", *Journal of Heat Transfer*, vol. 139, (1), p. 012 402, 2017.

[20] Kanchana C and Laroze D., "Study of chaos in rayleigh-benard convection of water-alumina nanofluid with heat source sink", *CU Journal of Non-Linear Fluid Mechanics*, vol. 1, (01), pp. 1–15, 2025.

[21] Siddheshwar P. G., Narayana M., Laroze D., and Kanchana C., "Brinkman–Bénard convection with rough boundaries and third-type thermal boundary conditions", *Symmetry*, vol. 15, (8), 2023.

[22] Firdose H., Siddheshwar P. G., and Idris R., "Effects of rough boundaries on Rayleigh–Bénard convection in nanofluids", *ASME Journal of Heat and Mass Transfer*, vol. 145, (6), p. 062 602, 2023.

[23] Kruthik P. S., Idris R., and Siddheshwar P. G., "Study of the linear and nonlinear regimes of natural convection with weak or dominating internal heat generation for rigid-free boundaries", *Journal of Porous Media*, vol. 28, (9), pp. 21–39, 2025.

[24] Bergman T. L., *Fundamentals of Heat and Mass Transfer*. New York, NY: John Wiley & Sons, 2011.

Data Availability

The authors declare that no data was generated.